Resolution enhancement of scanning four-point-probe measurements on two-dimensional systems.

Hansen, Torben Mikael; Stokbro, Kurt; Hansen, Ole; Hassenkam, T.; Shiraki, I.; Hasegawa, S.; Bøggild, Peter

Published in:
Review of Scientific Instruments

Link to article, DOI:
10.1063/1.1589161

Publication date:
2003

Document Version
Publisher's PDF, also known as Version of record

Resolution enhancement of scanning four-point-probe measurements on two-dimensional systems

Torben M. Hansen,[a] Kurt Stokbro, and Ole Hansen
Mikroelektronik Centret, Technical University of Denmark, Building 345e, DK-2800 Kgs. Lyngby, Denmark

Tue Hassenkam
Department of Chemistry, University of Copenhagen, Universitetsparken 5, DK-2100 Copenhagen E, Denmark

Ichiro Shiraki
AIST Tsukuba Central 4, 1-1-1 Higashi, Tsukuba, Ibaraki 305-8562, Japan

Shuji Hasegawa
Department of Physics, School of Science, University of Tokyo, 7-3-1 Hongo, Bunkyo-ku, Tokyo 113-0033, Japan

Peter Bøggild
Mikroelektronik Centret, Technical University of Denmark, Building 345e, DK-2800 Kgs. Lyngby, Denmark

(Received 17 February 2003; accepted 17 March 2003)

A method to improve the resolution of four-point-probe measurements of two-dimensional (2D) and quasi-2D systems is presented. By mapping the conductance on a dense grid around a target area and postprocessing the data, the resolution can be improved by a factor of approximately 50 to better than 1/15 of the four-point-probe electrode spacing. The real conductance sheet is simulated by a grid of discrete resistances, which is optimized by means of a standard optimization algorithm, until the simulated voltage-to-current ratios converges with the measurement. The method has been tested against simulated data as well as real measurements and is found to successfully deconvolute the four-point-probe measurements. In conjunction with a newly developed scanning four-point probe with electrode spacing of 1.1 μm, the method can resolve the conductivity with submicron resolution. © *2003 American Institute of Physics.* [DOI: 10.1063/1.1589161]

I. INTRODUCTION

With the emergence of nanostructured materials such as conducting polymers[1] and the continuing decrease of feature sizes of electronic circuitry, investigation of the conducting properties on a nano/submicron scale has become an important issue. For many decades, the four-point probe has been used to measure surface and bulk electrical conductivity in various materials. The near suppression of contact resistance makes interpretation of the measurements considerably easier than, for instance, spreading resistance and two-point measurements. The difficulty in bringing four individual electrodes close together, and the fact that the spatial resolution of the method is limited by the area in which the current flows through the sample, has until recently made the four-point measurement technique unsuitable for micro- and nanometer-scale investigations. The four-point probe is best suited for detection of spatial conductivity variations that are negligible over several times the electrode spacing. This is true for both linear and Hall electrode geometries.

Methods relying on a single moving tip, such as the scanning spreading resistance method,[2,3] and nanopotentiometry allow the electronic properties to be investigated with nanoscale resolution. The scanning spreading resistance measures the contact resistance between the probe and the sample. The outcome is however a complex combination of several factors including the contact area, Schottky barrier, surface states, contact pressure as well as the spreading resistance itself. The scanning potentiometer relies on the current being homogeneously distributed over the sample. To find the absolute local conductivity, the sample must be homogeneous on a macroscopic scale, as well as on an intermediate scale in the vicinity of the investigated area. Due to the typically large distance between the electrodes, for these two systems, a large fraction of the current runs in the bulk of the sample. Therefore, both the scanning spreading resistance and the scanning potentiometer are less sensitive to surface phenomena than the microfour-point probe.[4] Methods like scanning tunneling microscopy (STM) and scanning tunneling spectroscopy allow the electronic structure to be measured with atomic resolution, but do not directly measure the conductivity either.

Several groups have developed four-tip STMs that can perform four-point-probe measurements with electrode spacings down to 1 μm.[5] The complexity of these instruments and the difficulty in aligning the four tips individually has so far prevented mapping of the conductivity. Recently, linear microfour-point probes with electrode spacing down to 1.1 μm were developed on a single silicon chip.[6] The microfour-point probes have been used to map the conductivity on systems such as conductive polymers and surface reconstructions on silicon.[4,7,8] These systems exhibit structures on a

[a]Electronic mail: hansen.torben@nims.co.jp

nanoscale, which can be expected to influence the conductivity. To reduce further the electrode spacing, nonstandard fabrication techniques have to be employed.[9]

In this article, we present an altogether different route to obtain higher spatial resolution in four-point-probe measurements. If multiple four-point measurements are performed in a dense grid over the sample, then by numerical deconvolution of the data, a dramatic improvement of the resolution can be obtained. We demonstrate scanning measurements with a resolution of 1/15 of the electrode spacing, which is an improvement of nearly two orders of magnitude, as the resolution normally quoted for a four-point probe is roughly three times the electrode spacings.

II. METHODS AND RESULTS

A. Four-point resistivity at conductive sheets

The four-point probe consists of four electrodes arranged in an equidistant linear array. In the standard configuration, a current I is fed through the sample via the two outer electrodes. This generates a voltage drop V across the two inner electrodes, which is measured by a high impedance voltmeter. For a homogeneous two-dimensional (2D) conductive sheet with the sheet conductivity $G_{\square}$, the measured voltage-to-current ratio is given by[10]

$$\frac{I}{V}=\frac{\pi}{\ln 2}G_{\square}. \tag{1}$$

Analytical relations can only be found for homogeneous samples with simple geometries.[10,11] For inhomogeneous samples, the relation between the voltage-to-current ratio and the local conductivity becomes highly complex. In the following, we describe a numerical method for simulating the result of a four-point measurement for any arbitrarily varying 2D conducting sheet.

The simulation is then used to calculate the objective function for an optimization routine, that performs a fit of the simulated data to the measured data, to give a map of the real resistance.

Throughout this article, we will use the terms four-point resistivity and four-point conductivity meaning the resistivity or conductivity calculated from Eq. (1) using locally measured voltage-to-current ratios.

B. Convolution effect

To give an impression of the convolution effect of the four-point measurement, Fig. 1 shows a schematic of a four-point-probe scanning over a surface with a line defect of lower conductivity. The solid curve in Fig. 1 represents the real resistivity of the sample along the scanning line, while the dotted line represents the measured four-point resistivity. As can be seen, the feature in the four-point resistivity map is highly convoluted and appears to be much wider than the real feature. Also the conductivity level of the feature in the four-point resistivity map is not easily related to the conductivity of the real feature.

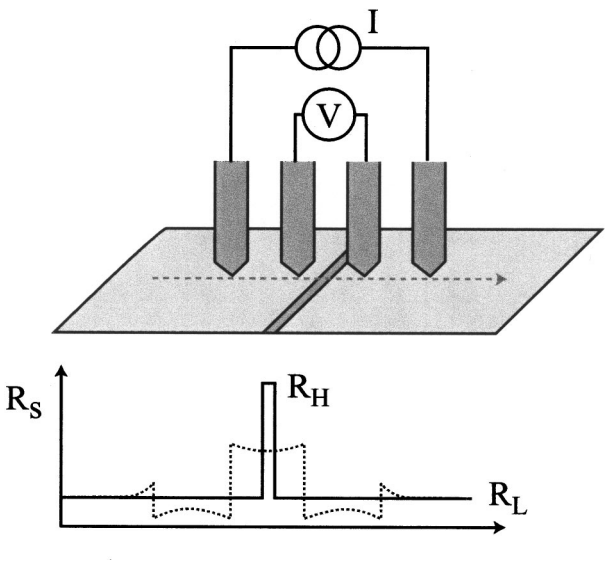

FIG. 1. Principle of scanning four-point measurement. The four-point probe is scanned in steps over the surface and for each step the voltage–current ratio is measured. The dark patch on the sheet indicates an area of increased resistivity. In the plot below, the solid line shows the resistivity and the dotted line the resulting voltage–current ratio as the probe is scanned over the surface.

C. Simulation of four-point resistivity maps

We want to simulate the cases of a four-point probe being scanned over a surface in equidistant steps in (a) the direction parallel to the probe orientation and (b) the direction perpendicular to the probe orientation.

The electrostatic potential in the sheet is given by the conservation equation

$$\nabla\cdot[\sigma(x,y)\nabla u(x,y)]=A[\delta(\mathbf{r}-\mathbf{r}_1)-\delta(\mathbf{r}-\mathbf{r}_2)], \tag{2}$$

where $\mathbf{r}_1$ and $\mathbf{r}_2$ are positions of the current source and the current drain, respectively. The current fed to the sample is denoted A. The local potential and sheet conductivity are denoted $u(x,y)$ and $\sigma(x,y)$, respectively. Equation (2) is discretized using the five-point finite difference formulation[12]

$$\begin{aligned}&G_{i-1/2,j}V_{i-1,j}+G_{i+1/2,j}V_{i+1,j}+G_{i,j-1/2}V_{i,j-1}\\&\quad+G_{i,j+1/2}V_{i,j+1}-(G_{i-1/2,j}+G_{i+1/2,j}\\&\quad+G_{i,j-1/2}+G_{i,j+1/2})V_{i,j}=I_{i,j},\end{aligned} \tag{3}$$

where $I_{i,j}$ is the total current fed in to grid block i,j:

$$\begin{aligned}I_{i,j}&=A\int_{\Delta x_{i,j}}dx\int_{\Delta y_{i,j}}dy[\delta(\mathbf{r}-\mathbf{r}_1)-\delta(\mathbf{r}-\mathbf{r}_2)]\\&=A(\delta_{i-i_1,j-j_1}-\delta_{i-i_2,j-j_2}),\end{aligned} \tag{4}$$

and $V_{i,j}$ is the potential at grid point $(i,j)=(x_i,y_j)$, see Fig. 2. The coefficient $G_{i+1/2,j}$ describes the conductance between grid point (i,j) and grid point $(i+1,j)$ given by the block centered method[13,14]

$$G_{i+1/2,j}=2\frac{\sigma_{i,j}\sigma_{i+1,j}\Delta y_j}{\sigma_{i+1,j}\Delta x_i+\sigma_{i,j}\Delta x_{i+1}}, \tag{5}$$

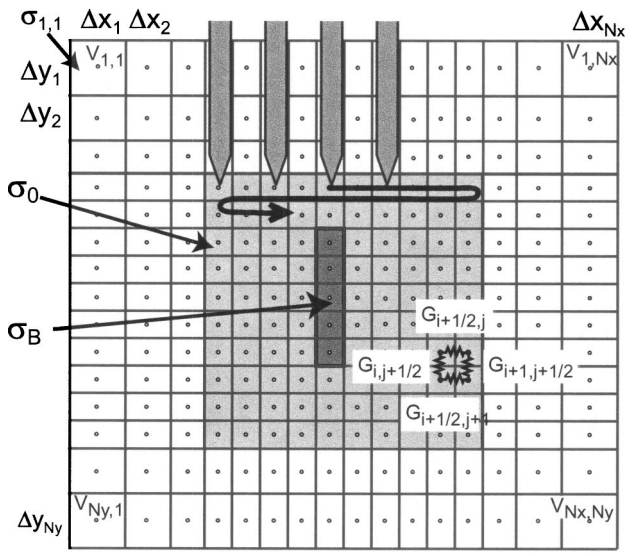

FIG. 2. Grid formation and model for four-point-probe simulation. The grid formation is the block centered formation. The small circles show the grid points and the rectangles show grid blocks. The conductors $G_{i+1/2,j}$, $G_{i,j+1/2}$, $G_{i+1,j+1/2}$, and $G_{i+1/2,j+1}$ show the conductor network equivalent.

where $\sigma_{i,j}$ is the average sheet conductivity in grid block (i,j) and Δx_i and Δy_j are the step sizes as shown in Fig. 2. $G_{i,j+1/2}$ is defined equivalently. $\delta_{i,j}$ is the discrete delta function.[15] In the area where the scanning is being performed, the grid points must coincide with the position of the electrode. Thus, the grid spacing must be an integer fraction of the electrode spacing. The electrode spacing is given by $s=n_x\Delta x_0+n_y\Delta y_0$ where Δx_0 and Δy_0 are the minimum grid spacings in the x and y directions, respectively.

The resulting set of equations can be written in matrix form

$$\mathbf{S}\mathbf{V}^k=\mathbf{I}^k, \tag{6}$$

where $\mathbf{V}^k$ and $\mathbf{I}^k$ are column vectors containing the N_xN_y values of $V_{i,j}$ and $I_{i,j}$, respectively, and the index k indicates the kth probe position. N_x and N_y is the number of grid points in the x and y directions, respectively. The node-admittance matrix $\mathbf{S}$[16] is given by

$$\mathbf{S}=\mathbf{A}_x\mathbf{G}_x\mathbf{A}_x^T+\mathbf{A}_y\mathbf{G}_y\mathbf{A}_y^T, \tag{7}$$

where $\mathbf{G}_x$ is a diagonal matrix containing the $N_x(N_y-1)$ values of $G_{i+1/2,j}$ and $\mathbf{G}_y$ contains the $(N_x-1)N_y$ values of $G_{i,j+1/2}$. $\mathbf{A}_x$ and $\mathbf{A}_y$ are the reduced incidence matrices[16] for the conductors directed along the x and the y axes, respectively. The incidence matrix relates a conductor with two grid points. If the conductance at $t_1=t(i+1/2,j)$ connects grid points $\ell_1=\ell(i,j)$ and $\ell_2=\ell(i+1,j)$ then $a^x_{\ell_1,t_1}=1$ and $a^x_{\ell_2,t_1}=-1$, where $a^x_{\ell,t}$ is the element in row ℓ and column t of $\mathbf{A}_x$ and $t(i+1/2,j)$ and $\ell(i,j)$ cast the grid index into a linear index.

The system of Eq. (6) then has to be solved for each probe position k in the four-point scan. For each new current vector $\mathbf{I}^k$, a new $\mathbf{V}^k$ is obtained. To extract the probe voltages, the potential vector $\mathbf{V}^k$ is multiplied with the vector $\mathbf{d}^k$:

$$V_p^k=(\mathbf{d}^k)^T\mathbf{V}^k. \tag{8}$$

The vector $\mathbf{d}^k$ contains only two nonzero elements so that

$$(\mathbf{d}^k)^T\mathbf{V}^k=V^k_{i_{p1},j_{p1}}-V^k_{i_{p2},j_{p2}}, \tag{9}$$

where (i_{p1},j_{p1}) and (i_{p2},j_{p2}) are the grid point indices at the position of the two inner electrode. The total system can now be written as

$$\mathbf{S}\mathbf{V}=\mathbf{I}, \tag{10a}$$

$$\mathbf{V}_p=\mathbf{d}^T\cdot\mathbf{V}, \tag{10b}$$

where $\cdot$ designates the diagonal of the matrix product. The columns of $\mathbf{V}$, $\mathbf{I}$, and $\mathbf{d}$ contain the vectors $\mathbf{V}^k$, $\mathbf{I}^k$, and $\mathbf{d}^k$, respectively. The vector $\mathbf{V}_p$ now contains the probe voltages for every probe position. The subscript p indicates the probe voltage difference as opposed to the node potentials $V^k_{i,j}$. When applying Dirichlet boundary conditions, the matrix $\mathbf{S}$ becomes a symmetric positive definite band matrix and the system can now efficiently be solved using the Cholesky method.[17] Due to the very large size of the right-hand side of Eq. (10a), indirect methods are generally not faster than the direct Cholesky method.

In order to bring the boundary as far away from the area of interest, without excessively increasing the number of free parameters, the grid spacing is gradually increased toward the edge of the simulation grid.

D. Deconvolution of four-point resistivity measurements

The aim of the deconvolution is to obtain the real conductivity of the sample from the measured data. Thus, we want to find the conductivity map that, through a simulation of the four-point measurement, leads to the best possible fit to the measured data. This requirement is equivalent to minimizing the objective function

$$E_0=\sum_k (V_p^k-V_m^k)^2, \tag{11}$$

with respect to the sheet conductivity map contained in the matrix σ. The measured voltages are given in V_m^k, while the voltages V_p^k are obtained by simulation as described in the previous section.

To efficiently optimize the system, we will need to know the gradient of the objective function and thereby the derivatives of the probe voltages with respect to the sheet conductivities. By using the so-called transpose system method,[18] we found that the dependence of the probe voltage V_p with respect to any parameter h influencing $\mathbf{S}$ can be written as

$$\frac{\partial V_p^k}{\partial h}=(\tilde{\mathbf{V}}^k)^T\frac{\partial \mathbf{S}}{\partial h}\mathbf{V}^k. \tag{12}$$

The transpose system voltages $\tilde{\mathbf{V}}^k$ are defined by

$$\mathbf{S}^T\tilde{\mathbf{V}}^k=-\mathbf{d}^k \quad \text{or} \quad \tilde{\mathbf{V}}^k=-(\mathbf{S}^{-1})^T\mathbf{d}^k. \tag{13}$$

For $\mathbf{S}$ being symmetric, we can write $\tilde{\mathbf{V}}^k=\mathbf{S}^{-1}(-\mathbf{d}^k)$ and the transposed system can be calculated together with the ordinary system as $[\tilde{\mathbf{V}},\mathbf{V}]=\mathbf{S}^{-1}[-\mathbf{d},\mathbf{I}]$, where the notation

$[\tilde{\mathbf{V}},\mathbf{V}]$ simply states that the columns of $\tilde{\mathbf{V}}$ precede the columns of $\mathbf{V}$ in one common matrix. The derivative of $\mathbf{S}$ with respect to $G_{i+1/2,j}$ is[18]

$$\frac{\partial \mathbf{S}}{\partial G_{i+1/2,j}} = (\mathbf{e}_{\ell(i,j)} - \mathbf{e}_{\ell(i+1,j)})(\mathbf{e}_{\ell(i,j)} - \mathbf{e}_{\ell(i+1,j)})^T, \tag{14}$$

where $\mathbf{e}_\ell$ is a unit element vector, with the ℓth element being 1 and all others are zero. $\ell(i,j)$ is the linear index of the node at (x_i, y_j). The derivative of the probe voltage for each conductor can then be written as

$$\frac{\partial V_p^k}{\partial G_{i+1/2,j}} = (\tilde{\mathbf{V}}^k)^T(\mathbf{e}_{\ell(i,j)} - \mathbf{e}_{\ell(i+1,j)})(\mathbf{e}_{\ell(i,j)} - \mathbf{e}_{\ell(i+1,j)})\mathbf{V}^k. \tag{15}$$

By the definition of $\mathbf{A}_x$, it can be seen that this is equivalent to

$$\frac{\partial V_p^k}{\partial \mathbf{G}_x} = ((\tilde{\mathbf{V}}^k)^T\mathbf{A}_x) * (\mathbf{A}_x^T\mathbf{V}^k), \tag{16}$$

where $*$ multiplies each element of two matrices of equal size, giving a new matrix of the same size. For the conductors in the y direction, it becomes

$$\frac{\partial V_p^k}{\partial \mathbf{G}_y} = ((\tilde{\mathbf{V}}^k)^T\mathbf{A}_y) * (\mathbf{A}_y^T\mathbf{V}^k). \tag{17}$$

Thus, we can write for the entire system

$$\frac{\partial \mathbf{V}_p}{\partial \boldsymbol{\sigma}} = (\tilde{\mathbf{V}}^T\mathbf{A}_x) * (\mathbf{A}_x^T\mathbf{V})\frac{\partial \mathbf{G}_x}{\partial \boldsymbol{\sigma}} + (\tilde{\mathbf{V}}^T\mathbf{A}_y) * (\mathbf{A}_y^T\mathbf{V})\frac{\partial \mathbf{G}_y}{\partial \boldsymbol{\sigma}}, \tag{18}$$

where $\partial \mathbf{G}_x / \partial \boldsymbol{\sigma}$ is the Jacobian for the collection of equations like Eq. (5) and equivalently for $\partial \mathbf{G}_y / \partial \boldsymbol{\sigma}$.

E. Suppression of false solutions

Now, in principle, we should be able to find the real conductivity of the sheet by a standard optimization routine with the objective function (11) and the Jacobian obtained from Eq. (18). However, since the maximum number of constrains V_m^k is $(N_x - 3n_x)(N_y - 3n_y)$, and the number of free parameters in $\boldsymbol{\sigma}$ is $N_x N_y$, the system is underdetermined. This means that in principle an infinity of different solutions exist which in many cases leads to oscillatory solutions.

An efficient way of suppressing such artifacts, is to introduce high-frequency penalty functions in the objective function. We use penalty functions given by

$$F^x_{\ell(i,j)} = f_f \frac{\sigma_{i,j} - \sigma_{i+1,j}}{\sigma_{i,j} + \sigma_{i+1,j}} \tag{19}$$

and

$$F^y_{\ell(i,j)} = f_f \frac{\sigma_{i,j} - \sigma_{i,j+1}}{\sigma_{i,j} + \sigma_{i,j+1}}, \tag{20}$$

where f_f is a weight factor. The Jacobi matrices are given as

$$\frac{\partial F^x_{\ell(i,j)}}{\partial \sigma_{p,q}} = \begin{cases} 2 f_f \dfrac{\sigma_{i+1,j}}{(\sigma_{i,j} + \sigma_{i+1,j})^2} & \text{for } p = i \text{ and } q = j \\ -2 f_f \dfrac{\sigma_{i,j}}{(\sigma_{i,j} + \sigma_{i+1,j})^2} & \text{for } p = i \text{ and } q = j+1 \\ 0 \quad \text{for all other values,} \end{cases} \tag{21}$$

and equivalently for $\mathbf{F}^y$. The new objective function becomes

$$E_h = E_0 + \sum_\ell F_\ell^{y^2} + F_\ell^{x^2}. \tag{22}$$

This function is minimized with respect to σ. A value of 0.1 for f_f was found to give reasonable results for a wide range of cases, and was chosen for all calculations in this work. The optimization routine used is a conjugated gradient based routine as implemented in MATLAB.

We will consider two simple cases: A step function corresponding to two neighboring domains of different conductivity and a delta function, corresponding to a high resistivity boundary separating two areas of similar resistivity. In both cases, we assume invariance in the direction perpendicular to the probe orientation.

A four-point measurement scan of the two domain case was calculated analytically. The two domains had sheet resistivities of 1 Ω and 10 Ω, respectively, and the electrode spacing was $s = 4\Delta x_0$. The result was deconvoluted for various values of f_f. The probe orientation was perpendicular to the step edge and the simulation grid had $M_x + 24 = 52$ by $M_y + 12 = 32$ internal grid points, where M_x and M_y are the numbers of evaluation points for the analytical result. The evaluation points were separated by a single grid point. The resulting resistivities for $f_f = 0.1$ are shown in Fig. 3(a). The outer ten rows and columns exhibit strong deviations from the correct result due to boundary effects and have been removed from the graphs shown. Apart from in these outer ten rows, the maximum error is approximately 15% for any weight factor between $f_f = 0.01$ and $f_f = 0.1$. For these weight factors, the step position is precisely established.

F. One-dimensional invariance

For systems being invariant in the y direction, these results can be greatly improved by also imposing invariant constrains for the deconvolution result. We then use only data from a four-point scan along a line in the x direction and the simulation is also done only for a single line. The conductivities are given by

$$\sigma_{i,j} = \sigma_i^y, \tag{23}$$

where σ_i^y is the conductivity in each line along the y direction and the Jacobian is given by

$$\frac{\partial V_p}{\partial \sigma_i^y} = \sum_{j=1}^{N_y} \frac{\partial V_p}{\partial \sigma_{i,j}}, \tag{24}$$

where $\partial V_p / \partial \sigma_{i,j}$ is given by Eq. (18) Due to the invariance in the y direction, larger grid spacings in this direction may be used. The result of deconvoluting a conductivity step from $1\ \Omega^{-1}$ to $0.01\ \Omega^{-1}$ is shown in Fig. 3(b) for electrode spac-

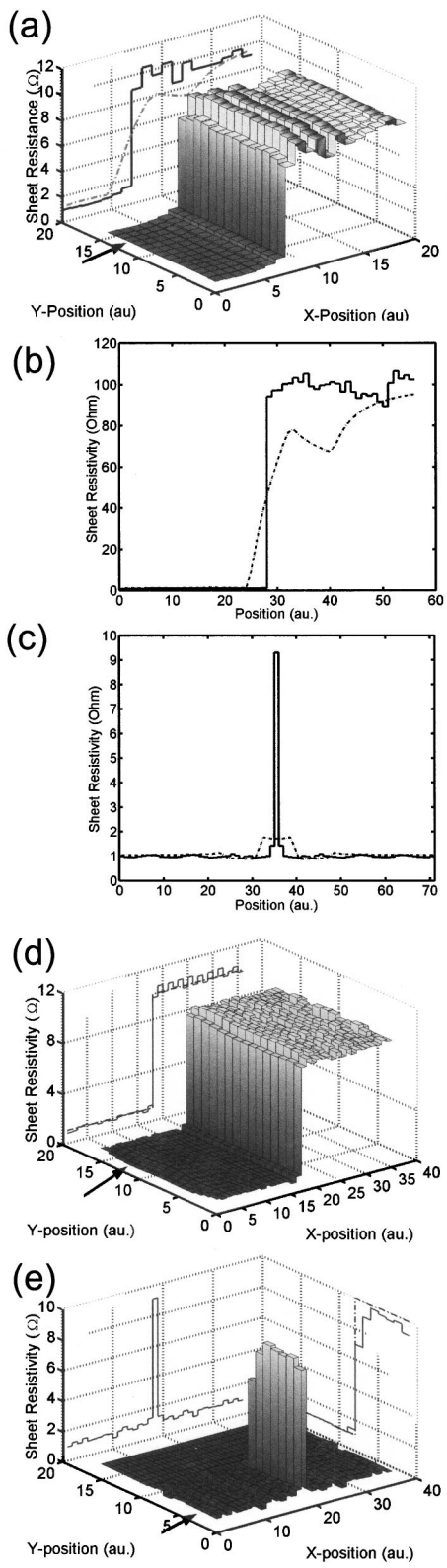

FIG. 3. (a) Deconvolution of analytical result for a step-function resistivity map. Low level: 1 Ω, high level: 10 Ω. The analytical four-point resistivity (dashed–dotted) and the poorest ($y=4$) deconvolution result (solid) is projected onto the backplane. The electrode spacing is $s=4\Delta x_0$. (b) Deconvoluted resistivity (solid) of analytically calculated four-point resistivity (dashed–dotted) with spacial invariance imposed in the direction perpendicular to probe orientation. Original resistivity has a step from 1 Ω to 100 Ω at $x=28$. Electrode spacing $s=8\Delta x_0$. (c) As (b) for a single Δx_0 wide 10 Ω peak on a 1 Ω background. (d) As (a) but using all principal configuration of the linear four-point probe and for $s=8\Delta x_0$. (e) As (d) for a Δx_0 wide peak penetrating only half way into the sheet.

ings $s=8\Delta x_0$ and penalty factors $f_f=0.1$. The grid size is 21 Δy_0 by $123\Delta x_0$ and we use $\Delta y_0=s$. For penalty factors from 0.01 to 0.1, the error is less than 10% and the step edge position is accurately reproduced.

Figure 3(c) shows the result of a similar calculation of a highly resistive boundary between two low resistivity domains. The errors are comparable to previous calculation.

G. Multiple four-point-probe configurations

The accuracy can be improved without penalty functions and any assumptions of invariance, by combining different voltage–current electrode configurations. Of the six possible configurations, three is sufficient to give unambiguous results. The model for these simulations is straightforward to derive from the aforementioned model by expanding the matrices **I** and **d**, to also include these other configurations.

We simulated four-point conductivity maps for the cases of (I) two neighboring domains with different conductivity and (II) a sheet of homogeneous conductivity with a highly resistive barrier penetrating half the area. In both cases, the four-point-probe orientation is perpendicular to the boundary. Figures 3(d) and 3(e) show the results of deconvoluting these maps. In both cases, the sharp features are retrieved to within 10% of the original conductivity map, as shown in the projections of the 2D data on the back plane of the graphs in Fig. 3 (marked with arrows). The original resistivity curves are marked with dashed lines, while the deconvoluted curves are marked with full lines.

III. RESULTS

The deconvolution method has been applied to a polymer system with artificially constructed defects. The system consists of a silicon sample with a 30 nm thick polythiophene film spun on top. Before spinning the polymer, trenches of approximately 2 μm width and approximate 2 μm depth were laser etched using the method described in Ref. 19. These trenches are seen as dark lines in the inset in Fig. 4(a).

A four-point measurement map was obtained by scanning a four-point probe, with an electrode spacing of 20 μm, over the sample in steps of 5 μm by 5 μm. From these measurements we have picked the result of a line scan along the white arrow in the inset of Fig. 4(a). Since the area can be considered translational invariant in the direction perpendicular to the probe orientation, we have used the method described in Sec. II F. In order to have the fitting errors in the same order as the penalty function response, the measurement values were normalized by dividing with 10^5 Ω before deconvolution. The simulation grid was 302 by 27. The grid spacing Δy_i of the simulation grid was $\Delta y_0=20$ μm for the innermost 11 grid blocks, increasing gradually to 500 μm at the edges along the x axis. The grid spacing Δx_i in the inner 286 grid blocks was $\Delta x_0=5$ μm increasing to 500 μm at the edge along the y axis. The penalty factor, f_f, was chosen to be 0.1. The central area of the deconvoluted resistivity map is shown in Fig. 4(a) (solid line) along with the original measurement (dashed line). The values have been renormalized by multiplying with 10^5 Ω.

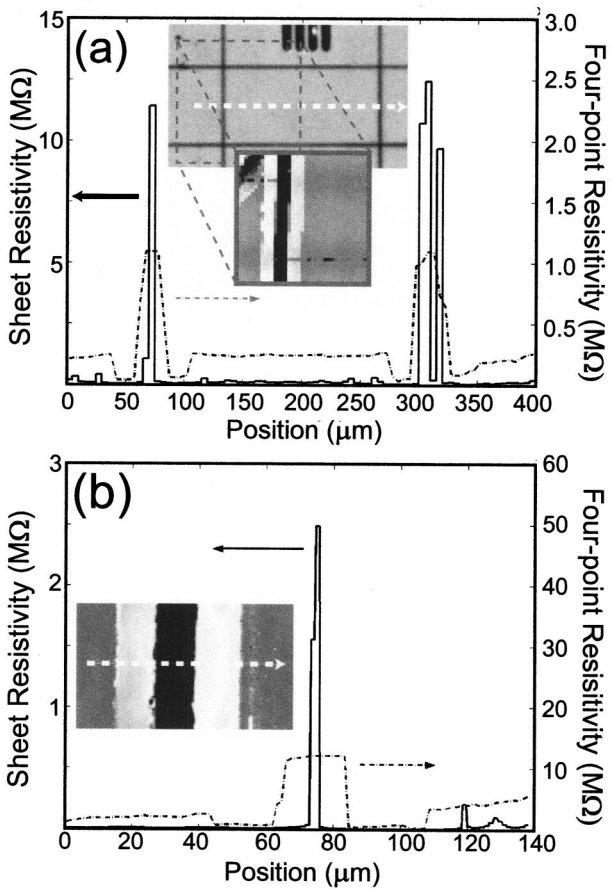

FIG. 4. (a) Deconvolution of a four-point scan along the line indicated by the arrow in the insert. The dashed–dotted line shows the measured four-point resistance, and the solid line shows the deconvoluted resistivity. The sample is prepared by laser etching trenches in silicon and subsequent spinning of a 30 nm thick conductive polymer. The splitting of the left-hand side peak is attributed to short circuiting over the trench by the probe contact. (b) Deconvolution of a scan similar to the one in (a) but with smaller step length. Again, the dashed–dotted line shows the measured four-point resistance and the solid line shows the deconvoluted resistivity.

A high-density scan of such a trench is shown in the inset of Fig. 4(b). In this case, the step size was only 1.3 μm. Using a simulation grid of 425 by 27, the trench is resolved as a sharp peak, just two grid spacings wide, as seen in Fig. 4(b). This has to be compared with the width of the etched trench of approximately 2 μm.

From these results, we can calculate the boundary conductivity, by which is meant the total conductivity across the boundary or defect. If we ignore the conductivity in the vicinity of the boundary, its conductivity per unit length can be calculated from

$$g_B = \frac{1}{\Sigma \rho_{s,i} \Delta x_i},$$

where the sum is over all the grid blocks that cover the boundary. The resistivity of the grid block is $\rho_{s,i}$ and Δx_i is the size of the grid block normally equal to Δx_0. For the two polymer systems, the boundary conductivity becomes $1.7 \times 10^{-2}\ \Omega^{-1}\,\mathrm{m}^{-1}$ and $1.5 \times 10^{-2}\ \Omega^{-1}\,\mathrm{m}^{-1}$ for the low-resolution (left-hand side boundary) and high-resolution maps, respectively. As these values are expected to be equal,

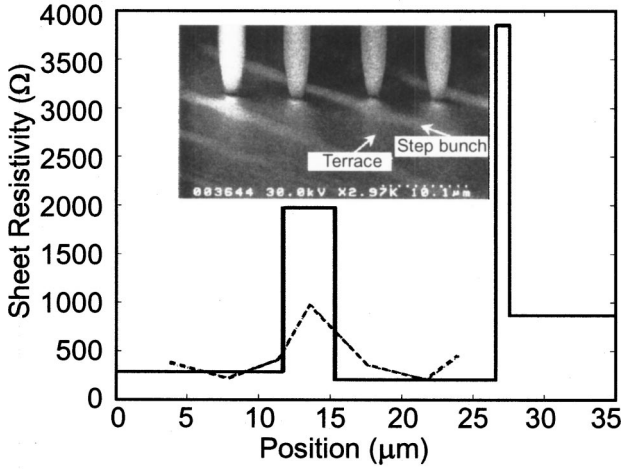

FIG. 5. Deconvolution of four-point resistivity measurements on a step-bunched Si(111)$\sqrt{3}\times\sqrt{3}$-Ag. The dashed–dotted line shows the measured four-point resistivities, and the solid line shows deconvoluted resistivity. Constant conductivity constraints are imposed on each area, i.e., step bands and terraces. The right-hand side most terrace is not sufficiently determined due to lack of measurements in the area. A scanning electron microscopy (SEM) pictures of a measurement on a similar sample is shown in the inset. The white bands are step bunches while the dark gray bands are terraces.

this can be taken as an indicator of the quality of the measurement and the deconvolution in combination.

Finally, we have applied the method to measurements on a step bunched Si$\sqrt{3}\times\sqrt{3}$-Ag surface. Four-point-probe measurements have been performed at various positions across the sample, in the direction perpendicular to the step bunches, using a 8 μm four-point probe at an angle of 45° with respect to the step bands. The changes in the voltage–current ratio depend on both the conductivity and the positions of the step bunches relative to the electrodes in a nontrivial fashion, similar to the case of the conductive polymer film. The experiment is described in detail in Ref. 8.

Because of the limited number of measurement points, the method was slightly modified for this particular case. The measured value is shown as a dashed–dotted line in Fig. 5. As seen in the scanning electron microscopy (SEM) micrograph insert the measurement area consists of terraces and step bands. By assuming the conductivity to be constant within each of these areas, we can modify the method in a manner similar to the one-dimensional translational invariant case. Thus, we have

$$\sigma_{i,j \in A_q} = \sigma_q^{sb} \quad \text{for} \quad q = 1, \ldots, m, \tag{25}$$

$$\frac{\partial V_p}{\partial \sigma_q^{sb}} = \sum_{i,j \in A_q} \frac{\partial V_p}{\partial \sigma_{i,j}}, \tag{26}$$

where σ_q^{sb} is the conductivity in area A_q and $i,j \in A_q$ represents all grid blocks inside the area A_q, the number of areas being m, and the area index being q. The measurement can be deconvoluted to give the result (solid line) shown in Fig. 5. The sheet resistivity of the terraces appear to be approximately 300 Ω, which is approximately the same as measured on a sample without step bunches. The resistivities of the step bunches appear to be much higher. The band A has a sheet resistivity around 2 kΩ while band B has a sheet resis-

tivity around 4 kΩ. This difference of a factor of 2 is easily explained by variations in step density. Also the high resistive step bunch is more narrow and thus is expected to have higher step density to accommodate for approximately the same height difference. The increased resistance of the right-hand sidemost terrace, compared to the other terraces, is an artifact due to a lack of measurements in the vicinity of the area.

IV. DISCUSSION

We have developed a method for obtaining the real resistivity map of 2D and quasi-2D systems, with a higher resolution than possible with a conventional four-point-probe technique. This was verified with data derived from analytical expressions for two cases of inhomogeneous resistivity landscapes. The original conductivity maps were retrieved with less than 10% error far away from transitions (domain and grid boundaries), and to within 15% near transitions.

For deconvolution of the measurement of the conductive polymer shown in Fig. 4(a), we see that the left-hand sidemost defect is almost perfectly resolved to just a single grid spacing. The measurements on the right-hand side defect give rise to a splitting of the deconvoluted peak. Because the defect is a trench in the sample the electrode drops into the trench and short circuits the defect which causes a significant measurement error. This error appears as a splitting in the deconvoluted resistivity plot. Since the defects are trenches, one may ask if the sample can still be considered two dimensional. The trenches however are shallow compared to the electrode pitch and an oxide layer between the silicon and the polymer prevents significant current from running through the bulk of the sample. As long as the electrodes are not located directly on top of the defect, the sample can thus be considered two dimensional.

In a few special geometries, the method is not applicable. If the conductivity along the probe orientation varies with a period, p, equal to the four-point-probe electrode spacing, s, the measured current–voltage will be independent of the position, thus the deconvolution will simply result in a constant resistivity map. This is also true for higher harmonics of the period, i.e., $p=s/n, n=1,2,3\ldots$. When the period is equal to the step size or its higher harmonics, the measurement is obviously independent of position and cannot be deconvoluted correctly. In the case of doubt, mapping using probes with different spacings on the same sample can be used as a verification of the measured data. Special cases, such as two closely spaced point defects and periodic conductance variation, will be investigated.[20]

The effective resolution of the four-point probe is highly dependent on the features of the conductivity landscape, and it is therefore difficult to establish a ''native'' resolution for a four-point probe. The resolution is ultimately limited by the size of the contact area, which must be significantly smaller than both the step size and the electrode spacing. The smallest electrode spacing reported for a four-point probe with fixed electrodes is 300 nm,[9] with contact areas of the order of 10 nm. Combined with the methods suggested in this article, resolutions of the order of 20–50 nm may be possible. This is a subject of further study.

The resolution obtained by the presented method does to some extent depend on resistance lamdscape. Specifically, the sample may contain harmonic components that the probe does not detect. In such cases, it is difficult to state an exact resolution for the method. Further investigations using different test models are necessary to clarify these aspects.

For semiconducting systems, the metal–semiconductor contact interface perturbs a much larger area due to band bending (Schottky contact), and therefore a poorer resolution of the four-point method should be expected for semiconductor systems. Alternatively, highly doped silicon probes could be used to measure on silicon surfaces, which could lead to nearly ohmic contacts. This would require the native oxide on both the probe and sample to be removed *in situ*, i.e., in the ultrahigh vacuum system prior to measurement. The contact phenomena could in principle be incorporated in the deconvolution method. However, because the admittance matrix would be changed at each contact position, it would have to be inverted every time, which would increase the amount of computational time tremendously.

One interesting feature of the model is the penalty function which, to a certain degree, allows the method to be customized. With low penalty factors, the height and positions of sharp features are reproduced accurately, whereas higher penalty factors effectively suppress oscillations in intermediate regions.

The method may be integrated with a four-point conductivity mapping station, so that nanoscale features are derived from resistance maps measured with microscale four-point probes. This could lead to new insight in the properties of electron transport in individual grains of thin metal films, surface state domains, and nanostructured systems.

ACKNOWLEDGMENTS

The authors would like to thank Hans Bruun Nielsen and Jakob Søndergård for help and fruitful discussions on optimization of ill-posed systems. They appreciate valuable discussions and comments on the manuscript from Antti-Pekka Jauho and Francois Gray.

[1] P. Bøggild, F. Grey, T. Hassenkam, D. R. Greve, and T. Bjørnholm, Adv. Mater. (Weinheim, Ger.) **12**, 947 (2000).
[2] P. De Wolf, T. Clarysse, W. Vandervorst, J. Snauwaert, and L. Hellemans, J. Vac. Sci. Technol. B **14**, 380 (1996).
[3] A. Malavé, E. Oesterschulze, W. Kulisch, T. Trenkler, T. Hantschel, and W. Vandervorst, Diamond Relat. Mater. **8**, 283 (1999).
[4] C. L. Petersen, F. Grey, I. Shiraki, and S. Hasegawa, Appl. Phys. Lett. **77**, 3782 (2000).
[5] I. Shiraki, F. Tanabe, R. Hobara, T. Nagao, and S. Hasegawa, Surf. Sci. **493**, 633 (2001).
[6] C. L. Petersen, T. M. Hansen, P. Bøggild, A. Boisen, O. Hansen, and F. Grey, Sens. Actuators A **96**, 53 (2002).
[7] I. Shiraki, T. Nagao, S. Hasegawa, C. L. Petersen, P. Bøggild, T. M. Hansen, and F. Grey, Surf. Rev. Lett. **7**, 533 (2000).
[8] S. Hasegawa, I. Shiraki, T. Tanikawa, C. L. Petersen, T. M. Hansen, P. Bøggild, and F. Grey, J. Phys.: Condens. Matter **14**, 8379 (2002).
[9] P. Bøggild, T. M. Hansen, O. Kuhn, F. Grey, T. Junno, and L. Montelius, Rev. Sci. Instrum. **71**, 2781 (2000).
[10] F. M. Smits, Bell Syst. Tech. J. **37**, 711 (1958).
[11] A. Uhlir, Bell Syst. Tech. J. **34**, 105 (1955).

[12] C. Jacoboni and P. Lugli, *The Monte Carlo Method for Semiconductor Device Simulation* (Springer, New York, 1989).
[13] E. C. Nacul and K. Aziz, Reservoir Eng. **Σ**, 37 (1991).
[14] The block centered method is also described in G. J. Hirasaki, *Lecture Notes for "Flow and Transport in Porous Media II Multidimensional Displacement"* (available at "http://www.owlnet.rice.edu/~ceng671/notes.htm"). It is here called "grid block formulation."
[15] A. W. M. Van den Enden and N. A. M. Verhoeckx, *Discrete-time Signal Processing* (Prentice–Hall, Englewood Cliffs, NJ, 1989).
[16] L. O. Chua, C. A. Desoer, and E. S. Kuh, *Linear and Nonlinear Circuits* (McGraw–Hill, New York, 1987).
[17] H. B. Nielsen and K. Madsen, *Løsning af lineære ligningssystemer* (Technical University of Denmark, 1972) (in Danish), Can also be found in various books on Numerical Analysis and Applied Mathematics.
[18] J. Vlach and K. Singhal, *Computer Methods for Circuit Analysis and Design*, 2nd ed. (Van Nostrand Reinhold, New York, 1994).
[19] M. Müllenborn, H. Dirac, and J. W. Petersen, Appl. Surf. Sci. **86**, 568 (1995).
[20] T. M. Hansen and P. Bøggild (unpublished).